Isı Bilimi ve Tekniği Dergisi, 35, 2, 1-18, 2015
J. of Thermal Science and Technology

ISSN 1300-3615

ARTIFICIAL NEURAL NETWORK BASED PREDICTION OF TIME-DEPENDENT BEHAVIOR FOR LID-DRIVEN CAVITY FLOWS

Akin PAKSOY* and Selin ARADAG**
*Turkish Petroleum Refineries Corporation (TUPRAS), R&D Center
Head Office, 41790 Korfez, Kocaeli, Turkey, akin.paksoy@tupras.com.tr
**TOBB University of Economics and Technology, Department of Mechanical Engineering
06560 Sogutozu, Ankara, Turkey, saradag@etu.edu.tr

(Geliş Tarihi: 08.07.2013, Kabul Tarihi: 09.09.2014)

Abstract: In this study, computational fluid dynamics (CFD) analyses of the two-dimensional, time-dependent lid-driven cavity flows, for Reynolds numbers ranging from 100 to 10000, are performed by using an in-house developed CFD code. The unsteady behavior of the flow is triggered using a sinusoidal lid velocity profile. The flow structure is further investigated with the application of a reduced order modeling technique, Proper Orthogonal Decomposition (POD), and the structures present in the flow, are separated according to their frequency (energy) content. POD results show that when the stream function formation is used as a data ensemble, about 99% of the total energy content can be modeled by considering only the most energetic first four POD modes; whereas, this value remains at a range between 90 – 95% for the x-direction velocity data ensemble. What is more, an Artificial Neural Network (ANN) based approach is developed to predict mode amplitudes for flows with different Reynolds numbers. Once enough information is obtained with the help of CFD of few flow cases, the ANN integrated approach presented herein helps to predict what is happening in the flow for different flow cases without requiring further CFD simulations, which are not practical in real-time flow control applications.
Keywords: Computational Fluid Dynamics, Time-dependent behavior, Cavity flow, Proper Orthogonal Decomposition, Flow control, Artificial Neural Networks.

KAPAK GÜDÜMLÜ KAVİTE AKIŞLARINDA ZAMANA BAĞLI DAVRANIŞIN YAPAY SİNİR AĞLARI TABANLI TAHMİNİ

Özet: Bu çalışmada, Reynolds sayısının 100 ile 10000 arasında değiştiği, iki boyutlu ve zamana bağlı kapak güdümlü kavite akışlarının Hesaplamalı Akışkanlar Dinamiği (HAD) çalışmaları özgün olarak geliştirilen HAD kodlarının uygulanmasıyla incelenmiştir. Akışın zamana bağımlı davranışı sinüssel hız profili uygulanarak tetiklenmiştir. Akış alanında gözlemlenen yapılar düşük boyutlu modelleme tekniği olan Dikgen Ayrıştırma Yöntemi (DAY) kullanılarak incelenmiş olup, bu yapılar frekans derecelerine (akış alanının bütününü ifade etmeye yönelik olan katkılarına, enerji içeriklerine) göre ayrıştırılmıştır. DAY sonuçlarına göre, akım fonksiyonu veri grubu olarak kullanıldığında, toplam enerji içeriğinin %99'a yakın kısmı sadece en yüksek enerji içeriğine sahip ilk dört DAY kipi kullanılarak ifade edilebilmektedir. Buna karşılık, x-yönündeki hız veri grubu kullanıldığında en yüksek enerji içeriğine sahip ilk dört kipin kullanılmasıyla toplam enerji içeriğinin % 90 – 95'lik bir kısmı ifade edilebilmektedir. Ayrıca, çalışmada değişik Reynolds sayılarının uygulandığı durumlar için Yapay Sinir Ağı (YSA) uygulaması yapılarak kip genlikleri de tahmin edilmiştir. HAD kullanılarak belirli akış durumları için yeterince bilgi toplandıktan sonra, YSA ile bütünleştirilen yaklaşım sayesinde farklı akış koşulları için gerçek zamanlı kontrol uygulamaları için pratik olmayan HAD analizlerine gerek duyulmadan akış alanında neler olduğuna ilişkin bilgileri tahmin etmek mümkün olmaktadır.
Anahtar Kelimeler: Hesaplamalı Akışkanlar Dinamiği, Zamana bağlı davranış, Kavite akışı, Dikgen Ayrıştırma Yöntemi, Akış kontrolü, Yapay sinir ağları.

NOMENCLATURE

$K_i(\vec{x})$	Modified data ensemble
M	Total number of snapshots
p	Pressure [Pa]
Re	Reynolds number [ρUD/μ]
T	Total number of time steps in one period
t	Actual time
u	X-direction velocity component [m/s]
$U_i(\vec{x})$	Original data ensemble of the physical activity
U_p	Moving lid velocity [m/s]
$U_p(t)$	Time-variant lid velocity [m/s]
v	X-direction velocity component [m/s]
$\vec{V}$	Velocity field
Δt	Numerical time step
ζ	Vorticity function
ψ	Stream function

INTRODUCTION

Driven cavity problem is one of the most popular fluid flow problems in Computational Fluid Dynamics (CFD). The availability of a simple geometry and boundary conditions, and capability of retaining relevant properties of several fluid flows such as boundary layers, eddies of different sizes and characteristics, and various instabilities (Peng *et al.*, 2003) make this problem eligible as a test case for the development of new simulation and solution methods to be applied in more complex flow problems.

In the literature, there are numerous studies based on driven cavity flows. For instance, Erturk *et al.* (2005) investigated numerical computations of the two-dimensional (2D) steady incompressible driven cavity flow based on Reynolds number (Re) with the range of $Re \leq 21000$. The authors provide a comparison for the different driven cavity studies in the literature. In another study performed by Perumal and Dass (2010), vortex patterns in a driven cavity is observed by moving both upper and lower horizontal boundaries together in parallel and anti-parallel directions for flows at Re ranging from 100 to 2000. Peng *et al.* (2003) worked on the direct numerical simulations of the transition process from laminar to chaotic flow in a lid-driven cavity problem. In an interesting study performed by Koblitz *et al.* (2010), the driven cavity problem is used as a validation case. The authors improved a previously developed in-house CFD code for 2D simulations including the effect of thermal stability in the atmospheric boundary layer for predicting geophysical transport phenomena.

For many of the engineering applications involving fluids, CFD plays a crucial role as one of the major tools to observe flow structures and their characteristics. On the other hand, for many practical approaches and realistic problems those involve fluids, CFD process remains expensive, time-consuming and resource-demanding (Gracia, 2010). Considering this, although CFD is counted as a valuable tool to obtain solutions for design and analysis purposes of complex thermo-fluidic systems, it lacks the functionality of being practical and quick for real-time or time-constrained applications. Such limitations cause difficulties especially in the development of flow control strategies (Fitzpatrick *et al.*, 2005).

To be fast enough in analyses to observe flow structures and their characteristics in a time-dependent system, a practical procedure is necessary to separate the space and time dependency of the system. Proper Orthogonal Decomposition (POD) is a statistical reduced order modeling technique which offers a lower dimensional model approximation to a given data ensemble obtained from computational or experimental studies (Paksoy *et al.*, 2011).

There are studies in the literature on application of the POD technique to construct low-dimensional models for lid-driven cavity flows. For example, in a study conducted by Gracia (2010), approximation errors are investigated by changing the extent of snapshots considered for the POD analysis of a 2D lid-driven cavity problem. In another study performed by Ahlman *et al.* (2002), driven cavity flow is used to enlighten to what extent POD can be successfully used to approximate time-dependent solutions of the incompressible Navier-Stokes equations with varying Reynolds number (Re) ranging from 10 to 2500. In a different research conducted for a Reynolds number Re=22000, Cazemier *et al.* (1998) successfully modeled the dynamics of a 2D driven cavity flow by representing 95% of the fluctuating kinetic energy of a direct numerical simulation data using the POD approach.

Theory behind the technique implies representation of large numbers of instantaneous characteristics of a dynamic system by a limited number of spatial and temporal structures, namely the coherent structures. A set of orthogonal basis functions and time-dependent coefficients are used for this purpose. They contain as much information as necessary to represent the original system dynamics by forming relevant POD modes. The representation is accomplished by considering an optimal amount of the most energetic POD modes. The approximation obtained by the POD technique contains adequate information to represent the original data ensemble with a reduced number of degrees of freedom (Ahlman *et al.*, 2002; Cazemier *et al.*, 1998).

The POD technique has been used widely for applications such as jet modeling, weather forecasting and operational oceanography, to obtain low dimensional descriptions of system dynamics by extracting dominant features and trends (Cao *et al.*, 2006). Lumley (1967) and Aubry *et al.* (1988) are the pioneers who utilized the statistical POD approach and low dimensional analysis in fluid flows. Lumley (1967) is the first person who employed the POD technique for the problems involving fluids interactions to obtain temporal and spatial characteristics of a flow field. As an extension of Lumley's studies, Aubry et al. (1988) modeled the wall region of a turbulent boundary layer using the features of the empirical eigenfunctions obtained as a result of the POD technique. The authors analyzed the chaotic turbulent flow dynamics of a realistic system by the POD technique to capture major flow characteristics as a low-dimensional model. As demonstrated in O'Donnell and Helenbrook (2007), Sen *et al.* (2007), Connell and Kulasiri (2005), Lieu *et al.* (2006), and several other studies in the literature utilize the POD technique in fluid mechanics applications as a reduced order modeling tool.

Artificial Neural Networks (ANN's) refer to computing systems the main idea of which is inspired from the analogy of information processing in biological nervous systems and human brain, where billions of neurons are interconnected to process a variety of complex information. A computational neural network works as a mathematical function which transforms a set of input variables into a set of output variables (Bishop, 1994). It consists of neurons as the simple processing units. In general, for systems that contain multiple inputs and

multiple outputs, a neural network structure contains two different layers, hidden and output layers, apart from the input layers. The neurons of each layer are interconnected with weights. Correct identification between a set of independent input variables and the output variables is obtained by changing the weight values (Khataee *et al.*, 2010).

Currently, neural networks are used for solution of problems in system identification, such as pattern recognition, data analysis, and control. ANN's have also been applied to diverse problems in several fields such as insurance, medicine, economic predictions, speech recognition and image processing. Several notable features of ANN's include relatively high processing speeds, learning ability of the solution of a problem from a set of examples, dealing with imprecise, noisy, and highly complex nonlinear data, and parallel processing ability (Nørgaard *et al.*, 2003). ANN's are also used effectively for fluid mechanical systems. For example, Zhang *et al.* (1996) used ANN's to estimate the flow characteristics observed in an elongated rectangular cross-sectional area of a static prism by considering two-dimensional von Karman vortex structures in the flow field. In another study, Ahadian *et al.* (2009) employed the ANN approach for modeling and prediction of the length of permeation in a nanochannel for two different types of fluids as a function of the influencing parameters, such as surface tension and viscosity of the fluids.

The objective of this study is to investigate time-dependent two dimensional flow structures and characteristics in a lid-driven cavity flow with the help of the POD technique and application of an ANN methodology to CFD simulation results. Computational data ensembles for the time-dependent two-dimensional driven cavity flows at different lid velocities are obtained by using an in-house developed CFD code for Reynolds numbers 100, 500, 1000, 5000 and 10000. The POD technique is used as a post-processing tool to analyze numerically obtained CFD data ensemble by identifying the most energetic modes (spatial components) and mode amplitudes (temporal components) according to their frequency contents.

The ANN approach is used to estimate the state of the flow for different lid velocities and to prepare a point of view for further flow control strategies. Prediction of the POD mode amplitudes is essential for that purpose. Therefore, the heuristically formed ANN structure is designed to work as a mathematical procedure by predicting new mode amplitudes for different lid velocities from specific lid velocity values under investigation and previously obtained POD mode amplitudes (a baseline case for which the CFD simulations have already been performed). This ANN integrated approach helps to predict what is happening in the flow without requiring further CFD simulations for several Reynolds numbers, which are computationally not practical in real-time flow control applications.

METHODOLOGY

Flow Field Simulation Methodology

The problem is on the flow dynamics of an incompressible fluid inside a square cavity. The vertical and lower horizontal boundaries of the cavity are set to meet no-slip condition. A time-dependent sinusoidal oscillating velocity function (U_p) is assigned as the upper horizontal boundary for the lid, which is assumed to have an infinite length. Figure 1 shows the schematic representation of the problem.

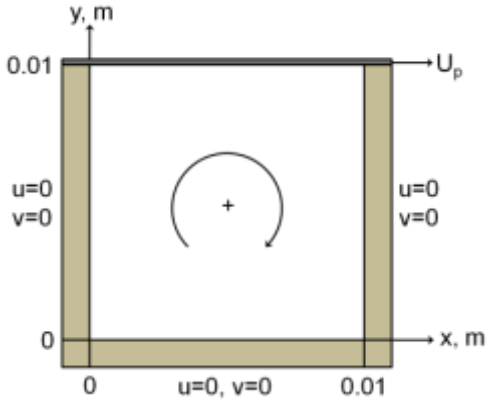

Figure 1. Schematic representation of the time-dependent two dimensional driven cavity problem.

During the numerical simulations, two-dimensional (2D) Navier-Stokes equations are solved. A vorticity-stream function formulation is used for the computations of the 2D flow in x-y plane as shown in Fig. 1. The velocity field is defined as $\vec{V} = (u, v)$ on the 2D bounded square domain with values $[0, 0.01\ \text{m}] \times [0, 0.01\ \text{m}]$. Kinematic viscosity of the fluid is taken as $1\times10^{-6}\ \text{m}^2/\text{s}$. For the domain where fluid is enclosed, incompressible Navier-Stokes equations and the continuity equation can be written as:

$$\frac{\partial \vec{V}}{\partial t} + \left(\vec{V}\cdot\nabla\right)\vec{V} = -\nabla p + \frac{\Delta \vec{V}}{\text{Re}} \tag{1}$$

$$\nabla \cdot \vec{V} = 0 \tag{2}$$

In Eq. (1), "$\vec{V}$" is the velocity field, "p" is the pressure and "Re" is the Reynolds number. By rewriting Eq. (1) in differential form for both velocity components for the 2D driven cavity problem Eq. (3) and Eq. (4) can be obtained.

$$\frac{\partial u}{\partial t} = -\frac{\partial u^2}{\partial x} - \frac{\partial uv}{\partial y} - \frac{\partial p}{\partial x} + \frac{1}{\text{Re}}\left(\frac{\partial^2 u}{\partial x^2} + \frac{\partial^2 v}{\partial y^2}\right) \tag{3}$$

$$\frac{\partial v}{\partial t} = -\frac{\partial v^2}{\partial y} - \frac{\partial uv}{\partial x} - \frac{\partial p}{\partial y} + \frac{1}{\text{Re}}\left(\frac{\partial^2 u}{\partial x^2} + \frac{\partial^2 v}{\partial y^2}\right) \tag{4}$$

In addition, the continuity equation is written as:

$$\frac{\partial u}{\partial x} + \frac{\partial v}{\partial y} = 0 \tag{5}$$

The vorticity and stream functions used in vorticity-stream function approach (Matyka, 2004) are shown by Eq. (6) and Eq. (7).

$$\zeta = |\zeta| = \left|\nabla \times \vec{V}\right| = \frac{\partial v}{\partial x} - \frac{\partial u}{\partial y} \tag{6}$$

$$\frac{\partial \psi}{\partial y} = u \quad and \quad \frac{\partial \psi}{\partial x} = -v \tag{7}$$

When the vorticity and stream function definitions given above are combined with Eq. (3) and Eq. (4), the pressure term is eliminated from the momentum equations. As a result of this combination, another form of the transport equation presented by Eq. (8) is revealed.

$$\frac{\partial \zeta}{\partial t} + u\frac{\partial \zeta}{\partial x} + v\frac{\partial \zeta}{\partial y} = \frac{1}{\mathrm{Re}}\left(\frac{\partial^2 \zeta}{\partial x^2} + \frac{\partial^2 \zeta}{\partial y^2}\right) \tag{8}$$

Combination of the Eq. (6) and Eq. (7) leads to acquisition of the Poisson equation as shown in Eq. (9) for the "ψ" variable.

$$\nabla^2 \psi = \frac{\partial^2 \psi}{\partial x^2} + \frac{\partial^2 \psi}{\partial y^2} = -\zeta \tag{9}$$

In the vorticity-stream function formulation, simple first order expressions for the derivatives of the vorticity, ζ, are defined at the wall boundaries. In addition, the stream function, "ψ", is set to zero at all boundaries. Then, for those boundaries defined to remain at the no-slip condition, the expression given by Eq. (10) is used, whereas, for the moving boundary the expression given by Eq. (11) is used where "U_p" is the moving lid velocity.

$$\zeta_{i,1} = \frac{2\left(\psi_{i,1} - \psi_{i,2}\right)}{\left(\Delta y\right)^2} \tag{10}$$

$$\zeta_{i,n} = \frac{2\left(\psi_{i,n} - \psi_{i,n-1}\right)}{\left(\Delta y\right)^2} - \frac{2U_p}{\Delta y} \tag{11}$$

After obtaining finite-difference equations for the vorticity transport equation with first order upwind differences for convective term, Alternating Direction Implicit (ADI) method is applied for the solution, while Point Successive Over-Relaxation (PSOR) method is used for the solution of the Poisson equation for the stream function. More information on these methods can be found in Tannehill *et al.* (1997).

In order to obtain the time-dependent data ensemble, the sinusoidal velocity profile of the lid is defined as:

$$U_p(t) = \left[\left(A\sin\frac{2\pi}{\Delta t \cdot T}t\right)B\right] \Big/ C \tag{12}$$

where "Δt" is the time step, "T" is the total number of time steps in one period of the simulation, "t" is the actual time, and A,B and C are arbitrary coefficients. These arbitrary parameters serve to retain the minimum lid velocity greater than zero and keep the maximum velocity value at desired limits. This is important, since Reynolds number is defined with a basis on the cavity height (0.01 m) and the maximum lid velocity.

There are totally five cases investigated in the numerical simulations of the 2D time-dependent driven cavity flow, at Reynolds numbers (Re) of 100, 500, 1000, 5000 and 10000. 10 complete sine cycles are simulated for each case. Hence, for 3000 time steps, there are totally 10 periods and each period contains 300 time steps. The parameters and maximum and minimum velocities for the analyzed Reynolds numbers are given in Table 1.

Table 1. Lid side velocity function parameters used in Eq. (12) and minimum and maximum velocities for all cases.

Re	Lid Side Velocity Function Parameters			Velocity (m/s)	
	A	B	C	Minimum $(\times 10^{-5})$	Maximum
100	0.999	1.001	200	1.0	0.01
500	0.999	1.000	40	2.5	0.05
1000	0.999	1.000	20	5.0	0.10
5000	0.999	1.001	4	50.0	0.50
10000	0.999	1.002	2	15.0	1.00

All the codes necessary to perform the numerical simulations are developed using Matlab. The CFD codes provide solutions at each time step for both velocity components of the 2D driven cavity flow, stream function, and vorticity values at each grid point.

The computational grid is generated by using quadratic grid elements for 101x101 (coarse), 201x201, and 301x301 (finer) grids. Before starting the unsteady simulations, each grid is tested with 3000 iterations for steady state simulations for a maximum of 1.00 m/s lid velocity. In Table 2, evaluated maximum stream function values are compared for each grid.

According to Table 2, it is seen that by improving the grid, maximum stream function value continues to evolve; however, this change is just about 5% between grids 101x101 and 301x301. Since the scope of this study is not based on obtaining very finely represented CFD simulations of detailed flow features, it is decided that the coarse 101x101 grid is eligible for further POD and ANN studies applied in the context of flow control purposes.

Table 2. Maximum stream function values for the tested grids with 3000 iterations at a Reynolds number 10000.

Grid	Maximum Stream Function Value
101x101	0.000440
201x201	0.000445
301x301	0.000416

POD Methodology

The POD technique is a statistical data analysis tool that is used for extracting dominant features and trends named as coherent structures that are typically patterns of space and time (Holmes *et al.*, 1996). In this study, the POD technique is used as a post-processing tool to analyze numerically obtained 2D driven cavity flow stream function and x-direction velocity data ensembles. The flow field observed in the cavity contains both spatial and temporal components. Utilization of the POD technique provides a relevant set of basis functions (also called as the modes) and mode amplitudes as a result of identification of the coherent structures depicted in the data ensembles. By projecting the governing Navier-Stokes equations, it is possible to mimic the physical behavior of the flow field accurately as a low-dimensional subspace model (Apacoglu *et al.*, 2011; Holmes *et al.*, 1996).

"$U_i(\vec{x})$" denotes a set of "M" observations including data of any property in the 2D cavity flow field taken at a position. Here, each observation is called a snapshot, and each snapshot represents the flow structures at one time step in time-dependent flow simulations. There is a debate in the literature about subtraction of the mean of data ensemble. Deane *et al.* (1991), Lall *et al.* (2002) and Newman (1996) suggested that the mean of the ensemble should be subtracted from the data ensemble to prevent further scaling requirements. However, Zhang *et al.* (2003) states that this approach provides no noticeable advantage for multiple data sets at different parameter values combined to generate a global reduced-order model.

In this study, the mean of the ensembles are subtracted to form new modified data ensembles as expressed in Eq. (13). POD is applied to two variables, the stream function and x-velocity.

$$K_i(\vec{x}) = U_i(\vec{x}) - \frac{1}{M}\sum_{i=1}^{M} U_i(\vec{x}) \qquad i = 1, 2, ..., M \qquad (13)$$

In the POD technique, modes are sorted out according to their energy content, which identifies the sheltering ability of the mode to portray original flow structures and their characteristics inside its formation. By projecting the governing Navier-Stokes equations, it is possible to mimic the physical behavior of the flow field accurately as a low-dimensional subspace model (Holmes *et al.*, 1996). Further detailed mathematical procedure for POD methodology is given in Ly and Tran (2001), and Sanghi and Hasan (2011).

ANN Methodology

In ANN, a neuron is a processing element that takes number of inputs, weighs them, sums them up, and uses the result as the argument for a singular valued function, which is called the activation function. The processing ability of the ANN is stored in the interunit connection strengths, or weights, obtained by a process of adaptation to, or learning from, a set of training patterns (Nørgaard *et al.*, 2003). Information about ANN fundamentals, network types and applications to different types of examples can be found in Haykin (1999), Mehrotra *et al.* (1996), and Samarasinghe (2006).

In this study, the system consists of multi inputs (namely the lid velocity data for five different cases observed at various Reynolds numbers and sampling mode amplitudes) and multi outputs (estimated mode amplitudes). Therefore, the ANN estimation method of choice includes application of Spatio-Temporal Time-Lagged (delayed) Multi Layer Perceptron (MLP) network structure, which is also named as Auto-Regressive, eXternal input (ARX), engaged ANN model system identification approach described by Nørgaard *et al.* (2003). This model includes nonlinear optimization techniques based on the Levenberg-Marquardt back propagation method.

The Levenberg-Marquardt method is a hybrid algorithm that combines advantages of the steepest descent and Gauss-Newton methods to produce a more efficient method than either of these two methods. It minimizes the difference between the extracted POD mode amplitudes and the ANN estimations, while adjusting the weights of the model (Samarasinghe, 2006).

The importance of the ARX engaged ANN dynamic network model structure is its strong stability capability even if the dynamic system under investigation is unstable. The stability is very important when dealing with nonlinear systems of partial differential equations, such as the Navier-Stokes equations (Siegel *et al.*, 2008). Further mathematical definition of the ARX-ANN model is given in Nørgaard *et al.* (2003) and Samarasinghe (2006).

By ANN application, it is needed to estimate mode amplitudes that are the same as the mode amplitudes obtained from the POD analyses utilized to the CFD results, but without using further CFD simulations. In this study, all the necessary ANN algorithms are coded using Matlab. In-house codes are used instead of built-in toolboxes.

RESULTS

Flow Field Numerical Simulation Results

The unsteady behavior of the flow field based on stream function data are shown in Fig. 2. Snapshots taken at 1300^{th}, 1400^{th} and 1500^{th} time steps falling into the half of the 10 periods are used to compare the flow structures and their characteristics in the 2D square cavity.

At first glance to Fig. 2, it is seen that the core region of the major vortex changes its place by moving closer to upper right corner of the cavity with increasing Reynolds numbers (Re). In addition, it is observed that the secondary flow structures exist at the bottom corners of the cavity for lower Reynolds numbers (Re), such as for Re=100 and Re=500. On the other hand, for rather higher Reynolds numbers, such as Re=1000, Re=5000 and

Re=10000, the secondary vortices do not expand widely at the corners, but they are scattered and confined to a smaller area on the vertical sides of the cavity. One reason of this is the application of increased lid velocities, and correspondingly, enhanced circulation of the fluid retained inside the flow field at higher Reynolds numbers. Another distinction that can significantly be expressed is that the major vortex formation dissipates for lower Reynolds numbers within time.

POD Application Results

The POD technique reveals the flow structures observed in the flow field of the 2D cavity. Both stream function and x-direction velocity data ensembles acquired for Reynolds numbers (Re) 100, 500, 1000, 5000 and 10000 are investigated by application of the POD technique for a total of 3000 snapshots. Each resulting POD mode carries certain spatial characteristic parts of the time-dependent physical behavior (either stream function or x-direction velocity formation) in the 2D square cavity flow field. For a good enough retention of the spatial characteristics and representation of the flow structures, it is adequate to consider a few most energetic POD modes.

Tables 3 and 4 show the energy content variation for the most energetic first four POD modes. As can be seen from those tables, most of the energy is accumulated in the first two POD modes of all cases for both stream function and x-direction velocity data analyses. When stream function data formation is taken into account, about 99% of the total energy content is revealed with consideration of the most energetic four POD modes. On the other hand, this value remains at a range between 90 – 95% for the x-direction velocity data formation cases. Since the stream function data ensembles retain the flow characteristics of both velocity components seen in the flow field, more behavioral activity can be kept for identification of the flow field during application of the POD technique.

Figure 3 shows time coefficient histories (mode amplitudes) for test cases at Re=100 and Re=10000. Mode amplitudes of each case represent temporal characteristics of the flow field. In Fig. 3a and Fig. 3c, for Reynolds number (Re) 100, which has the lowest maximum lid velocity and a velocity change in a narrower region compared to other cases, mode amplitudes shown by sinusoidal structures present a uniform periodical movement. The monotonic trend of the mode amplitudes seems to be still existing for the case at Re=10000. However, it is seen that in each of the 300 snapshots, which corresponds to one period in numerical flow simulations, the magnitudes of the mode amplitudes tend to change in a stepwise fashion. This can be clearly seen for all modes in Fig. 3b based on the stream function data analysis, and for modes 2, 3 and 4 in Fig. 3d based on the x-direction velocity data analysis. An identical attitude is also detected for Re=500, Re=1000 and Re=5000. The results shown in Fig. 3b and Fig. 3d are given as an illustration. The only change between the cases for Reynolds number (Re) 500, 1000, 5000, and 10000 is the maintained magnitudes of the mode amplitudes.

The uniform periodical movement observed for Re=100 and the stepwise monotonic attitude for other cases physically mean that there are major and secondary vortices formed in the flow field, and their formation intensities alternate with time. As an illustration, the most energetic four representative POD modes for stream function and x-direction velocity cases at Reynolds numbers (Re) of 100 and 10000 are shown in Fig. 4. In this figure, the spatial characteristics of vortex formation in the flow field are demonstrated. Since the amount of energy captured falls from mode 1 to mode 4, sizes of the vortices also decrease from mode 1 to mode 4. Besides, while the most energetic modes 1 and 2 in all cases exhibit the presence of a major vortex in the flow field, remaining modes show the existence of the secondary vortices scattered and confined in a rather small area in the flow field.

Figure 5 represents contours of the original and reconstructed stream function data ensembles for the snapshot number 1400 for Reynolds numbers (Re) 100 and 10000 using 4 modes. If infinite number of modes could be used during the reconstruction process of the flow field as a lower dimensional representation of the original one, it is clear that both of the results would exactly be the same. However, here, most of the flow is represented by only using 4 modes as opposed to infinite modes obtained from CFD simulations.

ANN Results

The utilized ANN procedure is able to estimate new mode amplitudes for different lid velocities and hence for different Reynolds numbers (Re) by employing a training process defined on a specific data set at a certain Re value.

Table 3. Energy contents of the most energetic first four POD modes of all test cases for stream function data analyses.

Mode Numbers	Energy Contents (%), Stream Function Data Analyses				
	Case 1 Re=100	Case 2 Re=500	Case 3 Re=1000	Case 4 Re=5000	Case 5 Re=10000
1	89.73	79.94	83.99	87.10	87.60
2	9.13	16.24	11.08	7.57	7.64
3	1.09	2.72	3.76	3.86	3.17
4	0.03	0.93	0.83	0.99	1.07
Total (4 Modes)	99.98	99.83	99.66	99.52	99.48

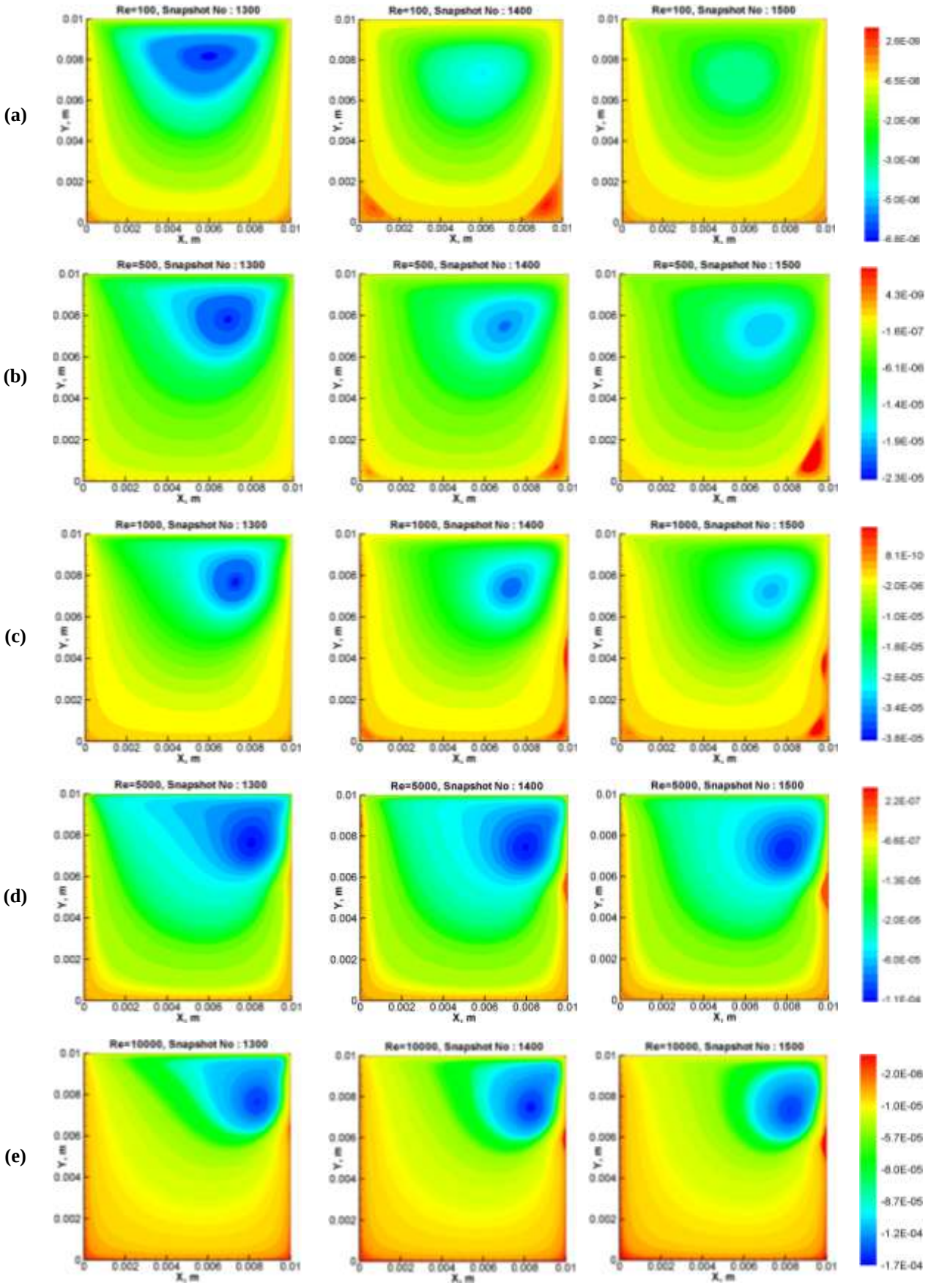

Figure 2. Unsteady solutions of the 2D lid-driven cavity flow field with a grid size of 101x101 observed for the test cases at (a) Re=100, (b) Re=500, (c) Re=1000, (d) Re=5000 and (e) Re=10000. Snapshots taken at 1300th, 1400th and 1500th time steps falling into the half of the 10 periods are used to compare the flow structures and their characteristics in the 2D square cavity.

Table 4. Energy contents of the most energetic first four POD modes of all test cases for x-direction velocity data analyses.

Mode Number	Energy Contents (%), X-Direction Velocity Data Analyses				
	Case 1 Re=100	Case 2 Re=500	Case 3 Re=1000	Case 4 Re=5000	Case 5 Re=10000
1	82.67	78.57	76.64	81.14	86.43
2	12.47	12.32	13.44	9.66	6.60
3	0.89	7.30	7.44	5.68	3.40
4	0.03	1.43	1.50	1.77	2.08
Total (4 Modes)	96.06	99.62	99.02	98.25	98.51

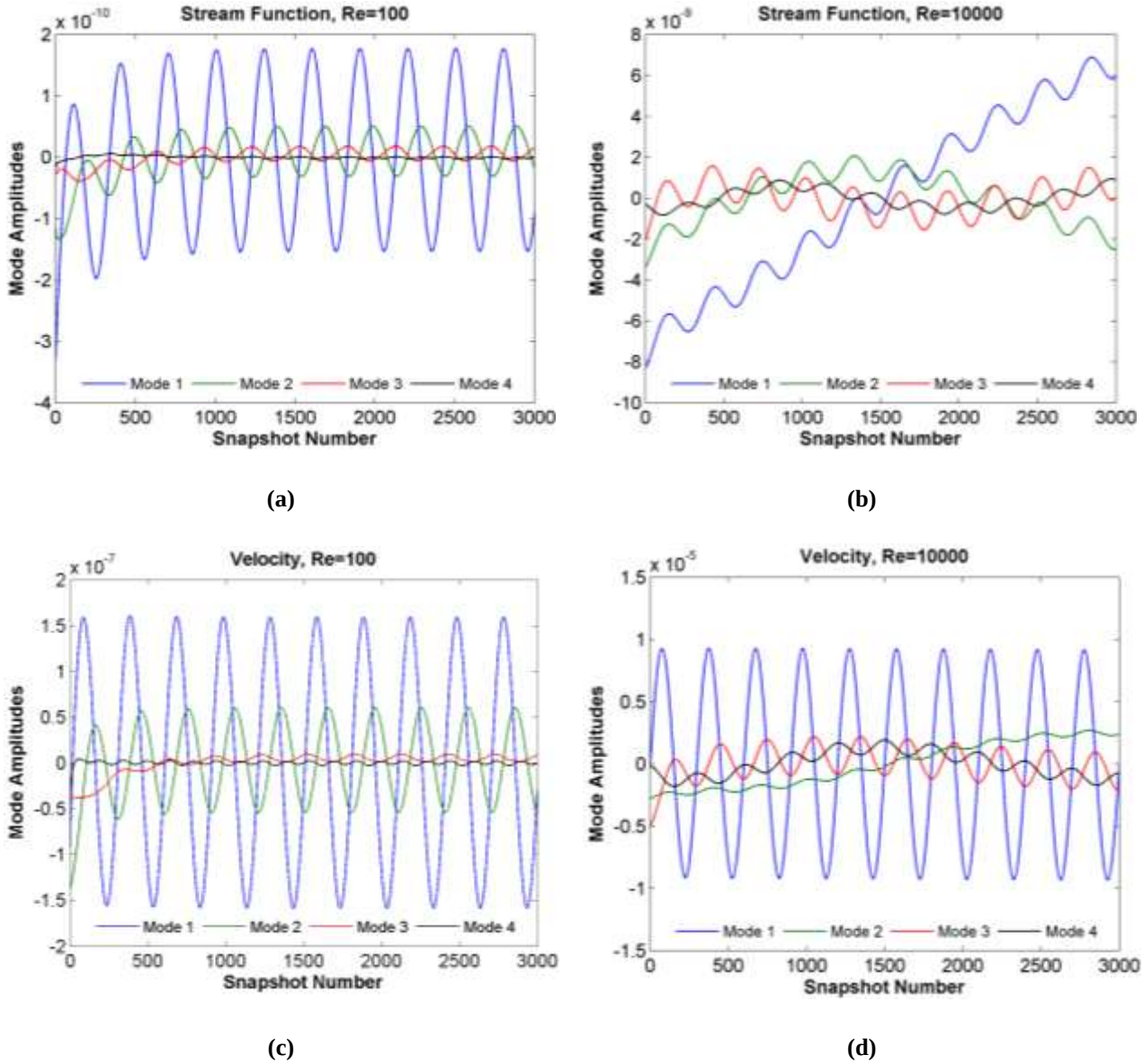

Figure 3. Snapshot number vs. mode amplitude change for the most energetic four POD modes of the stream function data analyzed test cases (a) for Re=100, and (b) for Re=10000; of the x-direction velocity data analyzed test cases (c) for Re=100, and (d) for Re=10000.

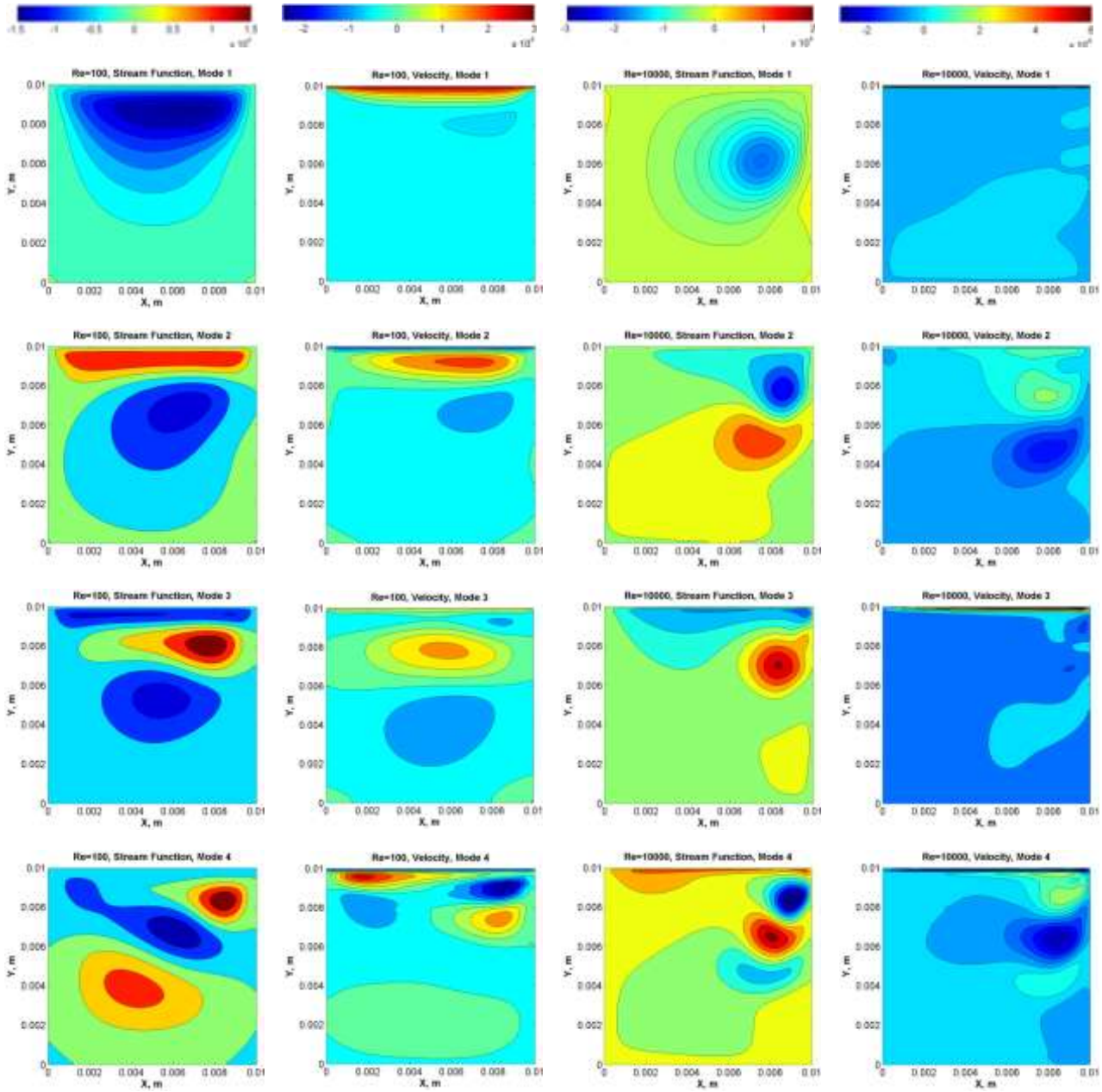

Figure 4. The most energetic four POD modes for (a) Re=100 stream function data analyzed, (b) Re=100 x-direction velocity data analyzed, (c) Re=10000 stream function data analyzed and (d) Re=10000 x-direction velocity data analyzed test cases.

Among a total of five cases established at Re values 100, 500, 1000, 5000 and 10000; Re=100 case is selected to determine and validate the network structure parameters. Whereas, Re=10000 case is selected as a baseline case to estimate mode amplitudes for the other cases with Re=500, Re=1000 and Re=5000.

The network is designed as a Spatio-Temporal Time-Lagged Multi Layer Perceptron (MLP) network in order to enable observation of the nonlinear relationship between multi inputs and multi outputs. The network structure consists of two layers (one hidden layer and one output layer) apart from the inputs section. There is only one hidden layer in the modeled network structure, and activation neuron function is based on the nonlinear tanh function. A single bias input has been added to the output from the hidden layer. The output layer has a linear activation function, and it consists of two outputs, namely mode amplitudes of the most energetic POD modes 1 and 2.

The problem under investigation is a real-time system application, and the use of ANN connected with ARX provides great harmony to observe such a dynamic real-time system via imposing the time delay parameter, which is an inherent parameter coming with the spatio-temporal time-lagged extension applied to the network.

During training process, the designed network uses a supervised learning approach with an adequate set of data. The training process employed in specification and validation of the network parameters (time delay and

hidden layer neuron number) uses mode amplitudes and time-variant lid velocities observed for Re=100 test case. The first half of the 10 periodic observations corresponding to 1500 time steps is used for training. The remaining data are estimated and used in the validation of the network structure.

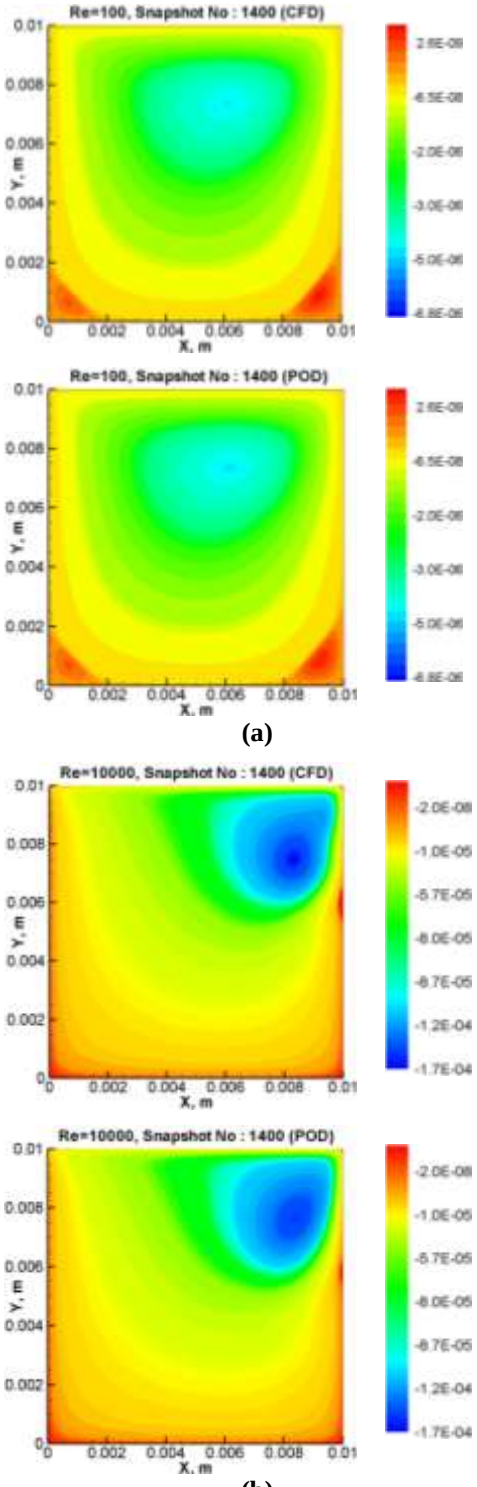

Figure 5. Original and reconstructed data for the 1400th snapshot by considering the most energetic four POD modes of stream function data analyzed test cases (a) for Re=100 and (b) for Re=10000.

Complexity and size of the network can be adjusted by varying both time delay and hidden layer neuron number parameters. Time delay value or the order of the lag length qualifies the number of mode amplitudes that need to be estimated and provided to the inputs section as data observed at the previous sampling instant in addition to the external time-variant lid velocity inputs for Re=100 test case. Hidden layer neuron number is another important parameter that influences prediction accuracy of the estimated mode amplitudes.

Accuracy and performance of the network are evaluated by monitoring estimation errors. The smaller the value of error, the better the forecast is. Considering this, deviation, R^2, root mean square (RMSE), mean absolute (MAE), and mean absolute percentage (MAPE) errors are calculated for the cases.

Performance measure tools of deviation, RMSE, MAE, and MAPE are expressed as:

$$\text{deviation} = \frac{T_t - z_t}{T_t} \tag{14}$$

$$\text{RMSE} = \sqrt{\frac{1}{n}\sum_{t=1}^{n}\left(z_t - T_t\right)^2} \tag{15}$$

$$\text{MAE} = \frac{1}{n}\sum_{t=1}^{n}\left|z_t - T_t\right| \tag{16}$$

$$\text{MAPE} = \frac{\sum_{t=1}^{n}\left|\frac{z_t - T_t}{T_t}\right|}{n} \times 100\% \tag{17}$$

where "z_t" is the network prediction value, and "T_t" is the corresponding target or observed value at an instant "t". Figure 6 presents network performance analysis results based on RMSE and MAE considered for stream function data group at Re=100, which is the network design and validation case.

To ascertain a feasible value for the time delay parameter, firstly, the network is analyzed by assigning an arbitrary constant hidden layer neuron number of 10, while time delay is changed from 2 to 10 with a step size of 2. According Fig. 6, an increase in time delay value positively affects accuracy of the results, and relatively decreases the order of the error signals. For larger time delay values, the network structure uses more known data as previous samples to train itself by interconnecting the input sets via setting up larger weighing matrices, and hence weights. RMSE does not provide a discernible approach for decision of the time delay parameter value. On the other hand, MAE of the changing time delays shows a difference less than 1% for the values 8 and 10. Therefore, it is decided to specify the time delay parameter value as 8. With this specification, there are 8 previous sampling histories of the mode amplitudes fed with the external time-variant lid velocity inputs to the network as input sets.

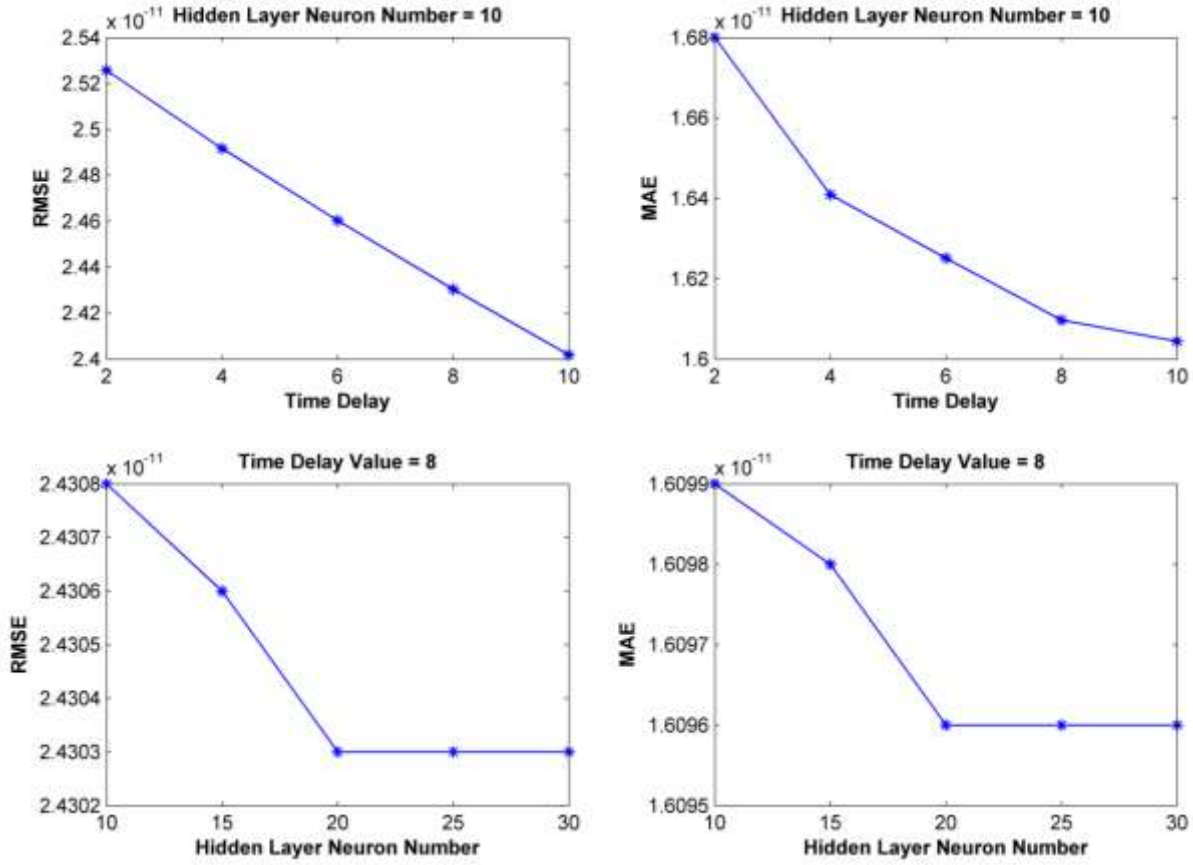

Figure 6. Network performance analysis results based on root mean square error (RMSE) and mean absolute error (MAE) applied to Re=100 stream function data used test case.

According to POD results, it is revealed that about 95% of the total energy content can be represented by using only the two most energetic POD modes (1 and 2) for the stream function formation. On the other hand, this value remains at about 90% for the x-direction velocity formation test cases. In either of the analysis cases, POD modes 1 and 2 retain most of the flow structures and their characteristics. Hence, estimation of the mode amplitudes constituting the major temporal behaviors of the flow is essential for further flow control purposes of such real-time application systems. In Fig. 7, ANN estimations of the mode amplitudes for modes 1 and 2, their comparison with the original POD evaluated data, and corresponding deviations are shown by utilizing the designed network structure for the test case at Re=100.

After ensuring the network structure, a heuristic approach is applied for ANN estimations of Re=500, Re=1000 and Re=5000 by selecting Re=10000 case as a baseline case. For the baseline case, 3000 time steps corresponding to the complete cycle of observations are used as the training data. The estimated results are compared with the original POD results at every 300 time steps for 10 periods. At the end of this process, 10 new significant data are obtained to scale estimated results to designate their monotonically changing patterns. This scaling process does not change the magnitudes of the estimated mode amplitudes, but assign their behavioral trend with respect to the original POD results.

The trained network structure with the mode amplitudes of the Re=10000 case is used for estimation of the mode amplitudes of the Reynolds numbers (Re) 500, 1000 and 5000. During this process just the time-variant lid velocity data is fed externally as an input set to the modeled network structure. During the estimation process, each estimated data set is multiplied with the mean average velocity of the external time-variant lid velocity input set and divided to the mean average velocity of the baseline Re=10000 case. Figures 8, 9, and 10 provides a comparison of the original and estimated mode amplitudes including deviations for Re=500, 1000, and 5000 for both stream function and x-direction velocity formations.

Among different error representation kinds, according to Emang *et al.* (2010), MAPE is a decisive error type in predictive analysis due to its understandable representation coming from the easy generic percentage term. Based on Lewis (1982), certain MAPE ranges representing various predictive model evaluations can be used to classify the quality of estimations. MAPE ranges and related accuracy settings defined by Lewis (1982) are given in Table 5.

It can be observed from Figures 7, 8, 9, and 10, resulting ANN estimations for mode amplitudes of modes 1 show adequate coherency with minor errors. On the other hand, for modes 2, the estimated outputs predict the similar periodical behavior observed for the POD results well enough but with a slight error in magnitude range.

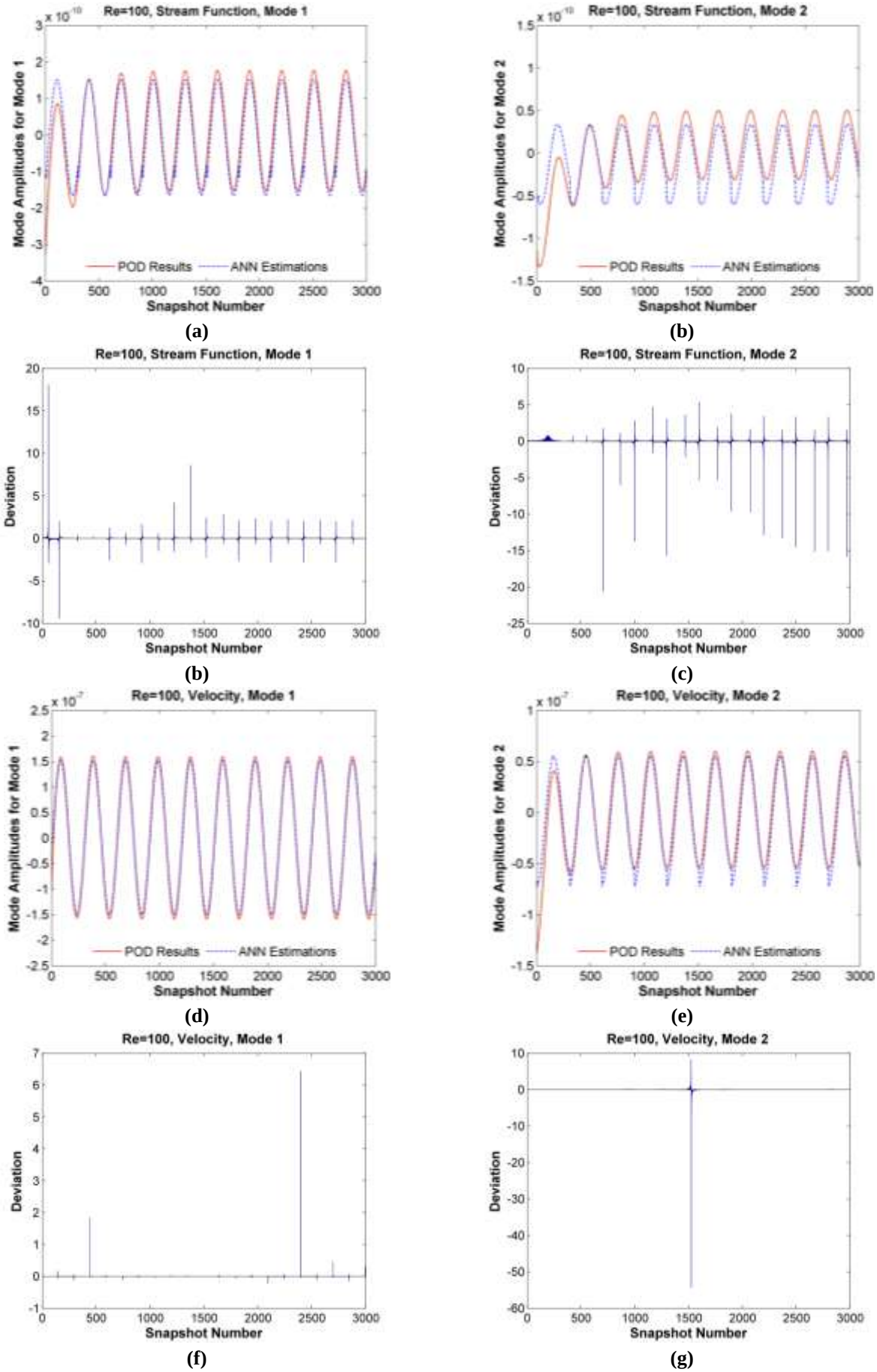

Figure 7. Comparison of original and estimated mode amplitudes for Re=100 test case, (a) and (b) for stream function, (e) and (f) for x-direction velocity data formation with their respective deviation plots (c,d,g and h).

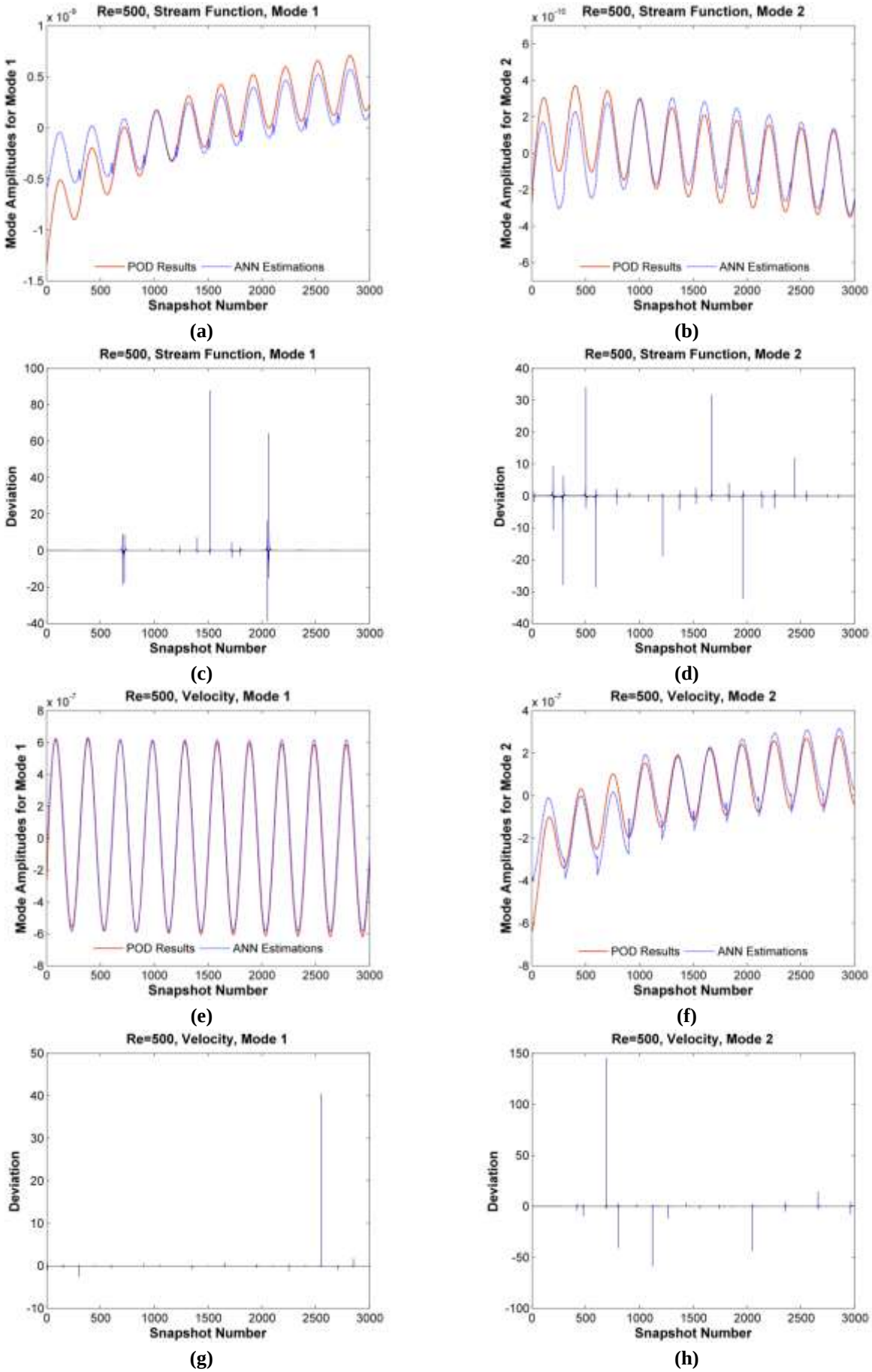

Figure 8. Comparison of original and estimated mode amplitudes for Re=500 test case, (a) and (b) for stream function, (e) and (f) for x-direction velocity data formation with their respective deviation plots (c,d,g and h).

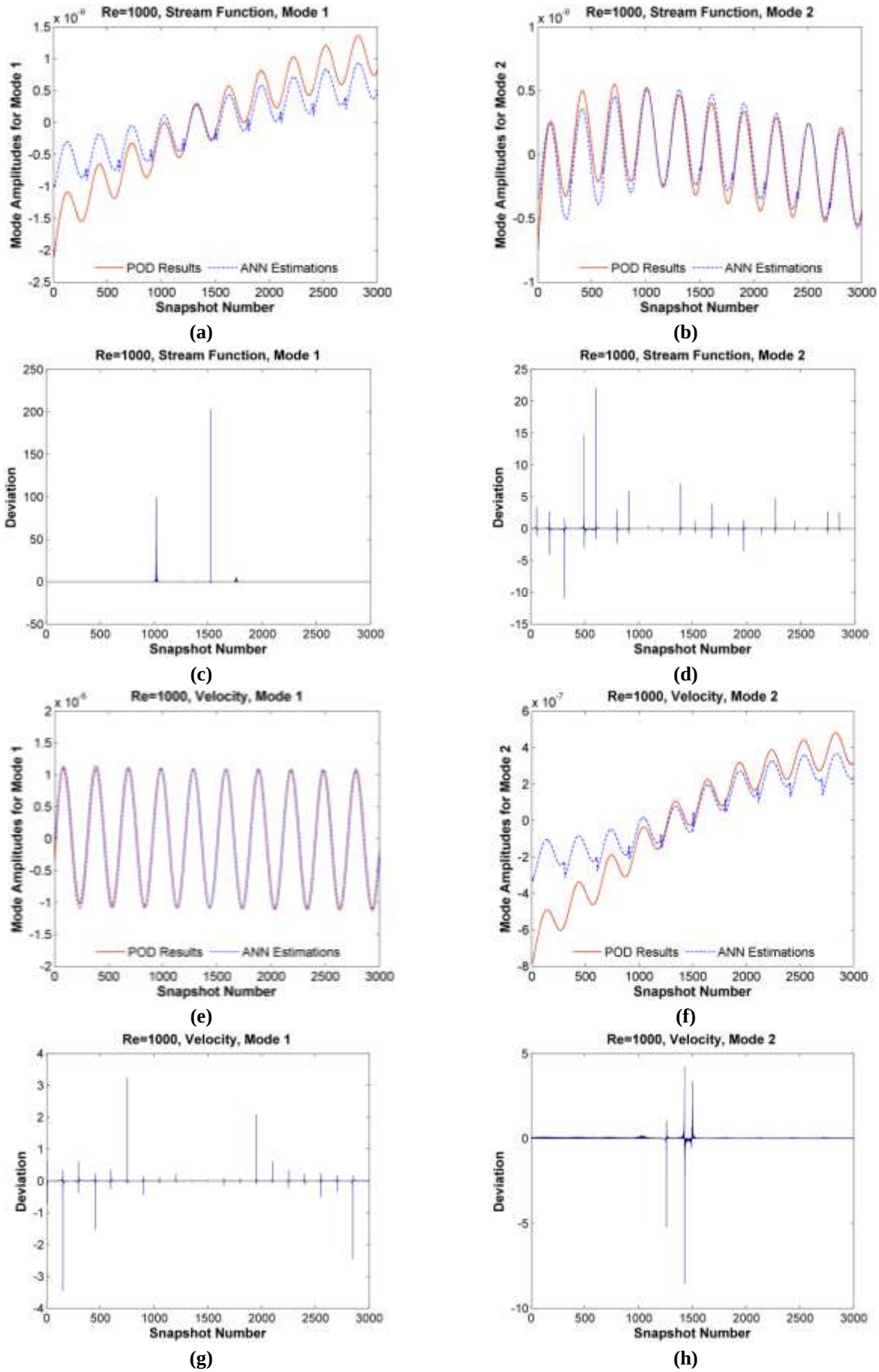

Figure 9. Comparison of original and estimated mode amplitudes for Re=1000 test case, (a) and (b) for stream function, (e) and (f) for x-direction velocity data formation with their respective deviation plots (c,d,g and h).

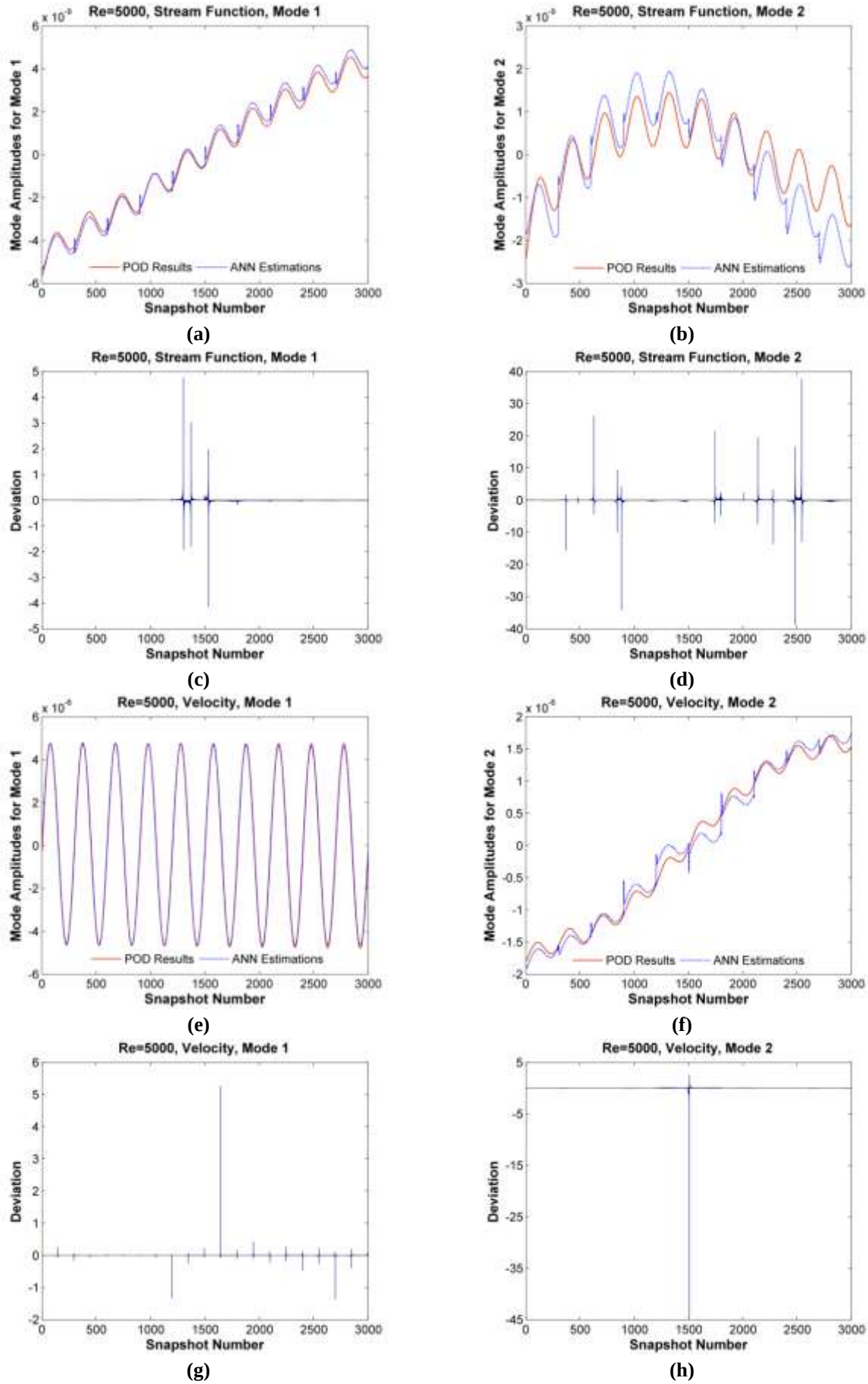

Figure 10. Comparison of original and estimated mode amplitudes for Re=5000 test case, (a) and (b) for stream function, (e) and (f) for x-direction velocity data formation with their respective deviation plots (c,d,g and h).

Tables 6, 7, 8, and 9 show R^2, RMSE, MAE, and MAPE values calculated for Re=100, 500, 1000, and 5000. Paying attention to MAPE results, it is seen that the network estimations are at high accuracy for modes 1 of x-direction velocity formations in all cases. There are reasonable outputs observed for stream function formations of Re=500 and Re=1000 cases. Although for some cases the constructed network structure catches trends but cannot manipulate amplitudes of the periodicity well enough, among 10 of 16 different prediction studies, according to MAPE results, the network structure forecasted the data in high accuracy with MAPE values lower than 10%.

Table 5. Typical MAPE values for prediction evaluation defined by Lewis (1982).

MAPE (%)	Forecasting Evaluation
$MAPE \leq 10\%$	High Accuracy
$10\% \leq MAPE \leq 20\%$	Good
$20\% \leq MAPE \leq 50\%$	Reasonable
$MAPE \geq 50\%$	Inaccurate

CONCLUSION

In this study, accurate enough CFD data is obtained for the unsteady solutions of two-dimensional (2D) driven cavity flows for Reynolds numbers (Re) 100, 500, 1000, 5000 and 10000 using vorticity-stream function formulation with a grid size of 101x101. To obtain the unsteady behavior, velocity of the moving upper boundary (lid) is assigned to change within time in a sinusoidal oscillating manner. The computational data ensembles for the time-dependent 2D driven cavity flows at different lid velocities are obtained by using an in-house developed CFD code for a total of 10 periods, where each period contains 300 time steps. The computed stream function and x-direction velocity component values at each grid point of flow field are considered for further POD and ANN applications.

POD technique is applied to the data ensembles in order to separate the spatial and temporal components of the flow by means of modes and mode amplitudes. The most energetic POD modes defining the vortical structures in the square flow field region of the 2D cavity reserve certain amount of the characteristics of the flow.

Table 6. R^2 values for modes 1 and 2 for both stream function (SF) and x-direction velocity data.

Mode #	Re=100		Re=500		Re=1000		Re=5000	
	SF	x-Velocity	SF	x-Velocity	SF	x-Velocity	SF	x-Velocity
1	0.935	0.996	0.882	0.997	0.941	0.990	0.997	0.999
2	0.819	0.987	0.811	0.893	0.922	0.863	0.858	0.989

Table 7. RMSE values for modes 1 and 2 for both stream function (SF) and x-direction velocity data.

Mode #	Re=100		Re=500		Re=1000		Re=5000	
	SF ($\times 10^{-12}$)	x-Velocity ($\times 10^{-7}$)	SF ($\times 10^{-11}$)	x-Velocity ($\times 10^{-9}$)	SF ($\times 10^{-11}$)	x-Velocity ($\times 10^{-9}$)	SF ($\times 10^{-11}$)	x-Velocity ($\times 10^{-9}$)
1	2.3302	4.4054	1.3961	1.9274	3.1193	2.7388	2.0659	5.8309
2	1.9577	1.5626	0.6670	4.4029	0.6586	11.6960	4.6655	10.3940

Table 8. MAE values for modes 1 and 2 for both stream function (SF) and x-direction velocity data.

Mode #	Re=100		Re=500		Re=1000		Re=5000	
	SF ($\times 10^{-12}$)	x-Velocity ($\times 10^{-7}$)	SF ($\times 10^{-11}$)	x-Velocity ($\times 10^{-9}$)	SF ($\times 10^{-10}$)	x-Velocity ($\times 10^{-8}$)	SF ($\times 10^{-10}$)	x-Velocity ($\times 10^{-8}$)
1	9.4683	1.6460	5.8198	6.9131	1.1862	1.0226	0.7557	2.2303
2	7.4382	0.6468	2.6056	17.8190	0.2601	5.0903	1.7663	3.9675

Table 9. MAPE values and accuracy definitions for modes 1 and 2 for both stream function (SF) and x-direction velocity data.

Mode #	Re=100		Re=500		Re=1000		Re=5000	
	SF	x-Velocity	SF	x-Velocity	SF	x-Velocity	SF	x-Velocity
1	8.06	0.51	21.67	2.82	28.03	1.45	2.50	0.80
	High	High	Reasonable	High	Reasonable	High	High	High
2	19.42	5.16	18.13	20.43	8.92	6.01	28.76	4.03
	Good	High	Good	Reasonable	High	High	Reasonable	High

By considering a few amount of energetic POD modes and related mode amplitudes, it is possible to mimic the retained physical behaviors obtained by CFD analyses with an adequate level of approximation. According to POD results, it is seen that more than 99% of the total energy content (frequency of the flow structures in the flow field) of the flows can be represented by using only four POD modes for the stream function data formation cases. On the other hand, this value remains at a range of 90 – 95% for the x-direction velocity data formation cases. The energy content of the modes decreases from mode 1 to mode 4. For lower Reynolds numbers (Re), such as Re=100, mode amplitudes present a periodically moving trend; however, for higher Reynolds numbers (Re), such as Re=10000, a monotonically changing (increasing or decreasing) trend is observed. The resulting modes and mode amplitudes of all test cases represent vortex formation and their evolution in time.

The spatio-temporal time-lagged Multi Layer Perceptron (MLP) network ANN structure with ARX extension is employed for prediction of the mode amplitudes for different lid velocities. The input set of the network consists of specific time-variant lid velocities that correspond to an investigated Reynolds number (Re) value and time delayed amount of POD mode amplitudes. The network structure uses training data of a baseline case for which the CFD simulations are performed, and estimates new mode amplitudes as outputs. With this ARX integrated ANN approach, a robust and real-time estimator of mode amplitudes which is necessary for observation of the effects flow structures and their characteristics in the flow field is evaluated effectively without requiring further CFD simulations.

ACKNOWLEDGEMENTS

This research is financially supported by Turkish Academy of Sciences Distinguished Young Scientists Awards Programme. (TUBA-GEBIP).

REFERENCES

Ahadian S., Mizuseki H. and Kawazoe Y., 2009, An Efficient Tool for Modeling and Predicting Fluid Flow in Nanochannels, *Journal of Chemical Physics*, 131.

Ahlman D., Söderlund F., Jackson J., Kurdila A. and Shyy W., 2002, Proper Orthogonal Decomposition for Time-Dependent Lid-Driven Cavity Flows, *Numerical Heat Transfer, Part B: Fundamentals*, 42, 285-306.

Apacoglu B., Paksoy A. and Aradag S., 2011, CFD Analysis and Reduced Order Modeling of Uncontrolled and Controlled Laminar Flow over a Circular Cylinder, *Engineering Applications of Computational Fluid Mechanics*, 5, 67-82.

Aubry N., Holmes P., Lumley J. L. and Stone E., 1988, The Dynamics of Coherent Structures in the Wall Region of a Turbulent Boundary Layer, *Journal of Fluid Mechanics*, 192, 115-173.

Bishop C. M., 1994, Neural Networks and Their Applications, Review Article, *Review of Scientific Instruments*, 65, 1803-1832.

Cao Y., Zhu J., Luo Z. and Navon I., 2006, Reduced Order Modeling of the Upper Tropical Pacific Ocean Model Using Proper Orthogonal Decomposition, *Computer and Mathematics with Applications*, 52, 1373-1386.

Cazemier W., Verstappen R. W. C. P. and Veldman A. E. P., 1998, Proper Orthogonal Decomposition and Low-Dimensional Models for Driven Cavity Flows, *Physics of Fluids*, 10 (7), 1685-1699.

Connell R. and Kulasiri D., 2005, Modeling Velocity Structures in Turbulent Floods Using Proper Orthogonal Decomposition, *International Congress on Modeling and Simulation*, Melbourne, Australia, 1237-1242.

Deane A. E., Kevrekidis I. G., Karniadakis G. E. and Orszag S. A., 1991, Low-Dimensional Models for Complex Geometry Flows: Application to Grooved Channels and Circular Cylinders, *Physics of Fluids*, 3, 2337-2354.

Emang D., Shitan M., Ghani A. N. A. and Noor K. M., 2010, Forecasting with Univariate Time Series Models: A Case of Export Demand for Peninsular Malaysia's Moulding and Chipboard, *Journal of Sustainable Development*, 3, 157-161.

Erturk E., Corke T. C. and Gokcol C., 2005, Numerical Solutions of 2-D Steady Incompressible Driven Cavity Flow at High Reynolds Numbers, *International Journal for Numerical Methods in Fluids*, 45, 747-774.

Fitzpatrick K., Feng Y., Lind R., Kurdila A. J. and Mikolaitis D. W., 2005, Flow Control in a Driven Cavity Incorporating Excitation Phase Differential, *Journal of Guidance, Control, and Dynamics*, 28, 63-70.

Gracia M. M., 2010, *Reduced Models to Calculate Stationary Solutions for the Lid-Driven Cavity Problem*, M.S. Thesis, Polytechnic University of Catalonia, Barcelona, Spain.

Haykin S., 1999, *Neural Networks: A Comprehensive Foundation* (Second Ed.), Prentice Hall, Upper Saddle River, NJ, USA.

Holmes P., Lumley J. L. and Berkooz G., 1996, *Turbulence, Coherent Structures, Dynamical Systems and Symmetry*, Cambridge University Press, Cambridge, UK.

Khataee A. R., Zarei M. and Pourhassan M., 2010, Bioremediation of Malachite Green from Contaminated Water by Three Microalgae: Neural Network Modeling, *Clean – Soil, Air, Water*, 38, 96-103.

Koblitz T. W., Bechmann A. and Sørensen N. N., 2010, The 2D Lid-Driven Cavity – Validation of CFD Code to Model Non-Neutral Atmospheric Boundary Layer Conditions, *Proceedings 6th PhD Seminar on Wind Energy in Europe*, Trondheim, Norway, 157-160.

Lall S., Marsden J. E. and Glavaski S., 2002, A Subspace Approach to Balanced Truncation for Model Reduction of Nonlinear Control Systems, *International Journal of Robust and Nonlinear Control*, 12, 519-535.

Lewis C. D., 1982, *International and Business Forecasting Methods*, London, Butterworths, UK.

Lieu T., Farhat C. and Lesoinne M., 2006, Reduced-Order Fluid/Structure Modeling of a Complete Aircraft Configuration, *Computer Methods in Applied Mechanics and Engineering*, 195, 5730-5742.

Lumley J. L., 1967, The Structure of Inhomogeneous Turbulent Flows, *Atmospheric Turbulence and Radio Propagation*, 166-178.

Ly H. and Tran H., 2001, Modeling and Control of Physical Processes Using Proper Orthogonal Decomposition, *Mathematical and Computer Modeling*, 33, 223-236.

Matyka M., 2004, *Solution to Two-Dimensional Incompressible Navier-Stokes Equations with SIMPLE, SIMPLER and Vorticity-Stream Function Approaches, Driven-Lid Cavity Problem: Solution and Visualization*, University of Wroclaw in Poland, Computational Physics Section of Theoretical Physics.

Mehrotra K., Mohan C.M., Ranka S., 1996, *Elements of Artificial Neural Networks (Complex Adaptive Systems)*, The MIT Press, Cambridge, MA, USA.

Newman A. J., 1996, *Model Reduction via the Karhunen-Loeve Expansion Part 2: Some Elementary Examples*, Institute for Systems Research, Technical Report No. 96-33.

Nørgaard M., Ravn O., Poulsen N. K. and Hansen L. K., 2003, *Neural Networks for Modeling and Control of Dynamic Systems*, Springer, UK.

O'Donnell B. J. and Helenbrook B. T., 2007, Proper Orthogonal Decomposition and Incompressible Flow: An Application to Particle Modeling, *Computers and Fluids*, 36, 1174-1186.

Paksoy A., Apacoglu B., and Aradag S., 2011, Reduced Order Modeling of a Turbulent Two Dimensional Cylinder Wake with Filtered POD and Artificial Neural Networks, *AIAA 49th Aerospace Sciences Meeting Including New Horizons Forum and Aerospace Exposition*, Orlando, FL, USA.

Peng Y. F., Shiau Y. H. and Hwang R. R., 2003, Transition in a 2-D Lid-Driven Cavity Flow, *Computers and Fluids*, 32, 337-352.

Perumal D. A. and Dass A. K., 2010, Simulation of Incompressible Flows in Two-Sided Lid-Driven Square Cavities, *CFD Letters*, 2, 13-24.

Sanghi S. and Hasan N., 2011 Proper Orthogonal Decomposition and Its Applications, *Asia-Pacific Journal of Chemical Engineering*, 6, 120-128.

Samarasinghe S., 2006, *Neural Networks for Applied Sciences and Engineering, From Fundamentals to Complex Pattern Recognition*, Auerbach Publications Taylor and Francis Group.

Sen M., Bhaganagar K. and Juttijudata V., 2007, Application of Proper Orthogonal Decomposition (POD) to Investigate a Turbulent Boundary Layer in a Channel with Rough Walls, *Journal of Turbulence*, 8, doi: 10.1080/14685240701615960.

Siegel S., Cohen K., Seidel J., Aradag S. and McLaughlin T., 2008, Low Dimensional Model Development Using Double Proper Orthogonal Decomposition and System Identification, *4th Flow Control Conference*, Seattle, USA.

Tannehill J. C., Anderson D. A. and Pletcher R. H., 1997, *Computational Fluid Mechanics and Heat Transfer* (Second Ed.), Taylor & Francis, Philadelphia, PA, USA.

Zhang L., Akiyama M., Huang K., Sugiyama H. and Ninomiya N., 1996, Estimation of Flow Patterns by Applying Artificial Neural Networks, *Information Intelligence and Systems*, 1-4, 1358-1363.

Zhang Y., Henson M. A. and Kevrekidis Y. G., 2003, Nonlinear Model Reduction for Dynamic Analysis of Cell Population Models, Chemical Engineering Science, 58, 429-445.

Akin PAKSOY

Akin Paksoy was born in Ankara in 1986. He received his BS degree from Hacettepe University, Department of Chemical Engineering in 2009, and his MS degree from TOBB University of Economics and Technology, Department of Mechanical Engineering in 2011. During his graduate studies at TOBB ETU, he worked as a research scholar in a project funded by The Scientific and Technological Research Council of Turkey (TUBITAK) to develop numerical methods and strategies for fluid flow and control applications. After graduation, he continued to work as a research assistant for about 2 years at Washington State University in a project funded by the Pacific Northwest National Laboratory for preparation and operation of sensors to investigate and visualize dynamic behavior of micro-scale systems. Currently, he is working as fluid and thermal systems modeling engineer at Turkish Petroleum Refineries Corporation (TUPRAS) R&D Center and advancing to get his PhD degree at Yeditepe University, Department of Mechanical Engineering.